Adaptive real-time architectures for phase-only correlation

Robert W. Cohn

A video-rate correlator can be constructed with a phase-only spatial light modulator and a CCD camera. The phase of the Fourier transform of a signal and a reference image is determined by fringe-scanning interferometry. The two measured phase images are then subtracted. The optical Fourier transform of this difference produces the phase-only correlation response. This system can update both signal and reference images with live scenery. Currently, only the joint transform correlator has demonstrated this degree of adaptivity in real time. Physically compact versions of the correlator can be built with a single spatial light modulator and a Fourier-transform lens.

Key words: Optical pattern recognition, phase-only filters, matched filtering, optical correlators, spatial light modulators, fringe-scanning interferometers.

Introduction

The mathematical operation of correlation is widely applicable to pattern recognition and to autonomous systems. Since the invention of the VanderLugt correlator,[1] there has been continuing research on developing coherent optical correlators that are adaptive and that perform one or more correlations at real-time video frame rates.[2] The term adaptive, as used by Yu *et al.*, implies that the reference signal/template can be changed automatically. They demonstrated a real-time and adaptive version of Weaver's and Goodman's joint transform correlator[3] (JTC), in which video-rate spatial light modulators (SLM's) represent the object-plane signals and the Fourier-plane hologram and video cameras serve as the holographic-detection medium and the correlation-plane detector. Yu's correlator can update the object plane with a new scene and reference signal during each frame. We refer to this characteristic as being adaptive in real time.

In both VanderLugt and joint transform correlators the nonlinearity inherent in the holographic recording process reduces the diffraction efficiency of the correlator.[4] In addition to the large amount of information contained in the phase, this observation on diffraction efficiency led Horner and Gianino to propose using a phase-only filter in place of the holographic matched filter in the VanderLugt correlator.[5] By canceling the phase variation of the signal across the filter plane while leaving the intensity unchanged, they demonstrated an improvement in diffraction efficiency of, at a minimum, 2.25×.

A real-time adaptive phase-only correlator requires not only a real-time phase-only SLM in the filter plane; it also requires that the SLM phase weights must be available in real time. The phase shift required of each pixel of the SLM can be calculated directly with the use of the fast-Fourier transform. The values of the phase weights can be computed off-line for a series of reference images and then stored in a multiframe video buffer. Many applications such as scene-based tracking and navigation do use live references (e.g., as in determining the frame-to-frame offset.) Knopp and Monroe have recently proposed using an interferometric technique to calculate the matched filter in the phase-only correlator in order to overcome this problem.[6] In their experimental demonstrations they determined only the sign of the phase. This permitted them to record three rather than four frames and greatly reduced the numerical processing in comparison with finding the analog values of phase.

We propose using a real-time electronic circuit that completely determines the analog phase from fringe-scanning interferometer measurements of the Fourier plane. This hybrid optical–electronic system suggests several variant correlator implementations that have the potential to demonstrate real-time adaptability and flexibility equivalent to that of the JTC.

The author is with the Department of Electrical Engineering, University of Louisville, Louisville, Kentucky 40292.

Received 24 February 1992.
0003-6935/93/050718-08$05.00/0.

General Description of Interferometer-Based Phase-Only Correlator

Figure 1 illustrates the correlation algorithm. Function blocks that can be associated directly with a physical analog are also identified, with the exception of the complex phasors between the lens and the camera. These are analogous to phase-shifted plane waves in the reference arm of an interferometer. Specific optoelectronic implementations derived from this flow chart are described below.

In Fig. 1 the signal $s(x, y)$ [and/or reference $r(x, y)$] is first Fourier transformed. The transform is interfered separately with the three phasors of known arguments ϕ_0, ϕ_1, and ϕ_2. The intensity $I_i(f_x, f_y)$ of the ith interference pattern is

$$\begin{aligned} I_i(f_x, f_y) &= |\exp(j\phi_i) + |S(f_x, f_y)|\exp[j\phi_S(f_x, f_y)]|^2 \\ &= 1 + |S(f_x, f_y)|^2 \\ &\quad + 2|S(f_x, f_y)|\cos[\phi_S(f_x, f_y) - \phi_i]. \end{aligned} \tag{1}$$

Measurements with the three reference phases set to $\phi_0 = 0$, ϕ_1, and $\phi_2 = -\phi_1$ permits the in-phase and quadrature components of the signal to be found by solving the two linear equations

$$\begin{aligned} I_0 - I_i &= 2|S|[\cos\phi_S(1 - \cos\phi_i) - \sin\phi_S \sin\phi_i] \\ &= I(1 - \cos\phi_i) - Q\sin\phi_i, \quad i = 1, 2 \end{aligned} \tag{2}$$

to yield

$$\begin{aligned} I &= \frac{2I_0 - I_1 - I_2}{2(1 - \cos\phi_1)}, \\ Q &= \frac{I_1 - I_2}{2\sin\phi_1}. \end{aligned} \tag{3}$$

The phase-estimation method is a special case of fringe-scanning interferometry[7] and may be compared with FM demodulation techniques.[8] These approaches use a phase shifter or a sine-wave oscillator that either continuously or discretely varies the reference phase from 0 to 2π. We choose to use the minimum number of discrete measurements in order to reduce data storage and to maximize processing speed.

In Eq. (3) both denominators are 2 if the phase arguments ϕ_0, ϕ_1, and ϕ_2 are set to 0, $\pi/2$, and $-\pi/2$ (which is illustrated specifically in Fig. 1.) An inverse-tangent circuit then converts the measurement of I and Q into an estimate of ϕ_S, the phase of the signal spectrum S. The phase estimate is subtracted from ϕ_R, the phase of the reference spectrum R. For a real-time adaptive correlator the reference phase would be determined by an identical interferometer. The transmittance of a phase-only SLM is set to the calculated values of phase ϕ. The SLM transmittance is optically transformed to yield the correlation-plane image

$$c(-x, -y) = \mathcal{F}\left[\frac{S(f_x, f_y)R^*(f_x, f_y)}{|S(f_x, f_y)R(f_x, f_y)|}\right]. \tag{4}$$

Equation (4) indicates that both the reference spectrum R and signal spectrum S are whitened in this system. The Horner–Gianino correlation whitens only the reference spectrum and leaves the signal spectrum unaltered.[5] A real-time adaptive version of their correlator would use only the interferometer to determine the phase of the reference R. Note that standard correlation can also be performed by using a tandem of a magnitude-only (in which magnitude is directly determined from I and Q) and a phase-only SLM.[9] However, the primary focus here is on phase-only correlators.

Phase-Only Spatial Light Modulators

Various liquid-crystal SLM's do exist that can approximate phase-only modulation.[10,11] A specific SLM that appears especially promising for phase-only spatial filtering is the flexure-beam deformable mirror device (FBDMD).[12,13] It is being developed at Texas Instruments under contract to the U.S. Defense Advanced Research Projects Agency.[14] The FBDMD consists of a 128 × 128 array of 46 μm × 46 μm micromechanical mirrors on 50-μm centers. Each

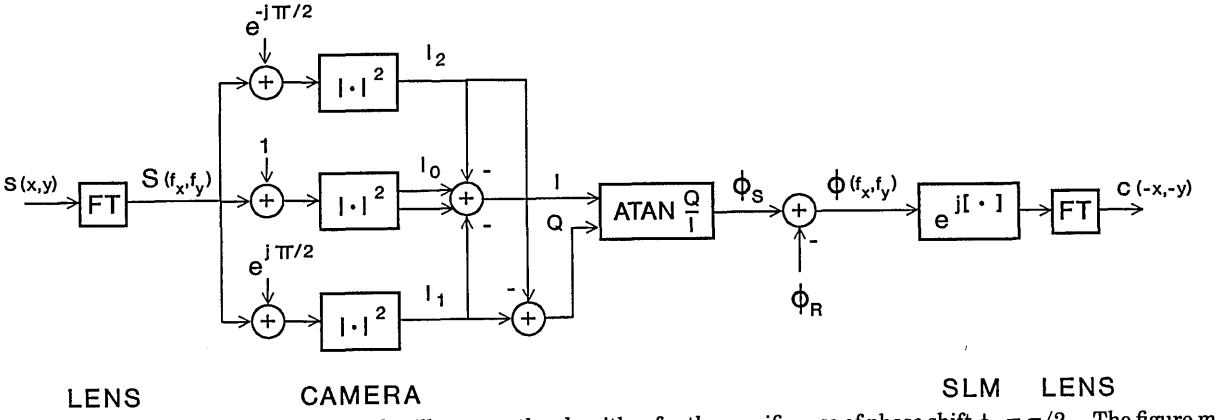

Fig. 1. Phase-only correlation algorithm. This illustrates the algorithm for the specific case of phase shift $\phi_1 = \pi/2$. The figure may be generalized by scaling I and Q by the factors found in Eq. (3). The case of $\phi_1 = 2\pi/3$ is also discussed in this study. FT's, Fourier transform operations; ATAN, inverse tangent.

mirror is suspended over an individually addressable field plate that deflects the mirror in a piston motion through electrostatic attraction. Experiments with individual pixels have demonstrated a range of 4π phase retardation for visible-wavelength light.[12] A deformable mirror device (DMD) (with a cantilever beam and tilt-producing micromechanical mirrors) has already been integrated on top of the same addressing circuit and demonstrated.[15,16] Pixellated piston-only SLM's can be set to approximate closely the phase of any wave front if the spatial variation of the wave front is less than the Nyquist rate (i.e., its phase varies by less than π rad/pixel.)

Opto-Electronic Implementations

Figure 2 illustrates a hybrid electronic–optic implementation of the correlation system. The front optics system is a Mach–Zehnder interferometer. The SLM transmittance is proportional to the real-valued video and reference signals $s(x, y)$ and $r(x, y)$. The Fourier transform of a signal is interfered with a reference beam. Phase shifting of the reference beam could be done with a transparent rotating wheel that is segmented into three different thicknesses, a piezoelectric mirror, or an electro-optic crystal. In the back optical system, the phase retardation of the phase-only SLM is set to the values $\phi(i, j)$, and the Fourier transform of the SLM transmittance is recorded by the camera.

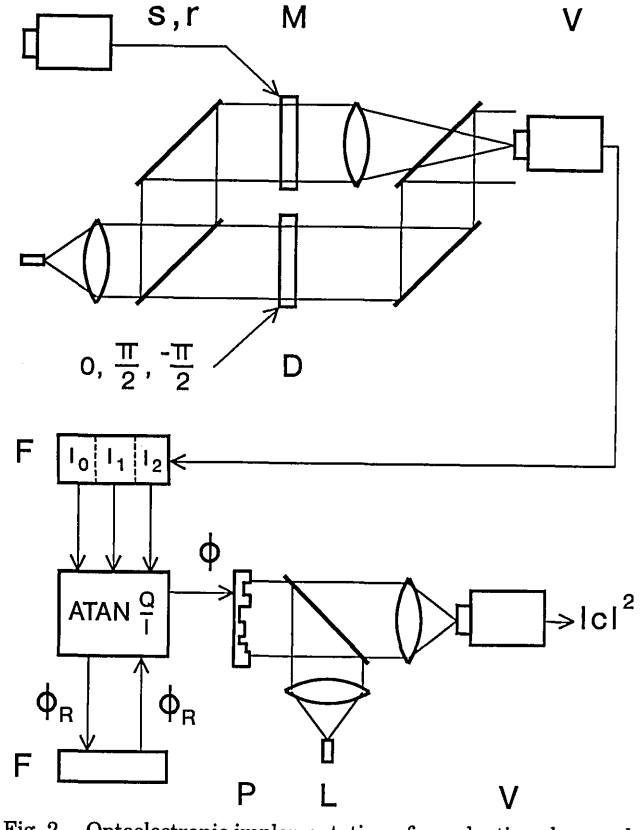

Fig. 2. Optoelectronic implementation of an adaptive phase-only correlator: M, magnitude-only SLM; V, video cameras; D, phase shifter; F, video frame memories; P, phase-only SLM (drawn as a reflective FBDMD); L, laser. In this implementation the phase for scene and reference signals time share the interferometer. The phase of the reference spectrum is stored in frame memory, and then, after the phase of the scene spectrum is calculated, the two phases are subtracted.

In this configuration a small amount of electronics has been used to reduce the amount of optical hardware in both the front and back optical systems. In the back system the electronic subtraction of the two phases replaces the step of optically multiplying transmittances $\exp(j\phi_S)$ and $\exp(j\phi_R)$ and thus eliminates the need for a second phase-only SLM. In the front system the magnitude-only SLM is first programmed with the reference signal and the video camera records the three interferograms; then the SLM is programmed with the scene signal, and three more interferograms are recorded. While the second set of interferograms is recorded the phase of the reference signal is calculated and stored in the lower of the two frame memories. As soon as the last scene interferogram is recorded, the calculation of the scene's phase and the simultaneous subtraction of the reference's phase is initiated. Thus the specific implementation in Fig. 2 illustrates that substantial optical hardware reduction is possible, though at a cost in electronic complexity. Furthermore, for this correlator to be adaptive in real time the internal electronics needs to process the six interferograms at the scene frame rate, even though only one optical transform of the phase-only SLM is needed per scene.

The Mach–Zehnder interferometer was chosen in order to eliminate all tilt from the reference beam. Tilt can cause rapid spatial variation of the interferogram, which would be averaged out by the large fill-factor pixels of most CCD cameras. It is therefore important to keep the spatial variation of the interferogram to below the Nyquist frequency of the image. If detectors of infinitesimal extent (which can be approached in practice by placing a sampling mask over the detector array) or an imager that oversamples the image are used, then a tilted reference can be used to illuminate the camera. This eliminates the need for the beam splitter immediately in front of the camera. As opposed to JTC and VanderLugt correlators, which also produce autocorrelation and convolution products, tilt or linear phase modulation is not required to separate these products.

Physically compact implementations are currently desired for many systems. Recent JTC demonstrations have achieved smaller size by using a single SLM, a lens, and a camera for both recording and reconstruction steps of the correlation process[2,16,17] Figure 3 illustrates an approach for making our phase-only correlator more compact. The optical system performs common-path interferometry of the phase-only SLM. The video scene and the reference image, here represented by the real signals $g(x, y)$ and $h(x, y)$, are nonlinearly transformed by the phase-only SLM into the complex-valued optical signals $s(x, y) = \exp[jg(x, y)]$ and $r(x, y) = \exp[jh(x, y)]$. The six frames used to determine the phase difference $\phi(i, j)$

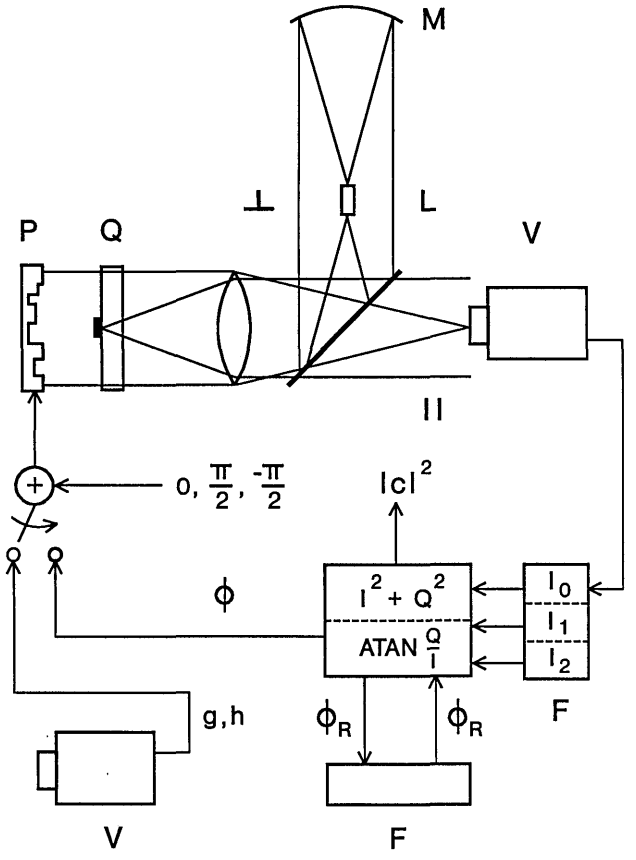

Fig. 3. Compact energy-efficient implementation of an adaptive phase-only correlator: M, curved mirror; L, laser diode (radiating from front and back facets); P, phase-only SLM; Q, quarter-wave plate; V, video cameras; F's, video frame memories. The quarter-wave plate has a mirror of small area deposited on its front surface. The quarter-wave plate and the polarized beam splitter are used together to efficiently direct light from the laser illuminator to the video camera. The SLM P also performs the function of phase shifting.

between S and R are presented to the SLM and processed by the inverse-tangent circuit in the same order as the Fig. 2 implementation. The phase-shifting operation is performed by offsetting the phase of each SLM pixel by 0, $\pi/2$, and $-\pi/2$ in successive frames. This follows from the linearity of the Fourier transform; in this case the Fourier transform is linearly scaled by a complex (and unit-magnitude) constant.

The nonlinear transform of the scene by the SLM may reduce the performance of the correlator below that obtained by using a magnitude-only SLM. Magnitude-only performance may be approximated by small phase-modulation depth or by binary phase-only modulation; specifically, binary thresholding of the scene followed by mapping of pixels above threshold to 1 (0 rad) and below threshold to -1 (π rad). The first mapping strategy leaves a large dc peak in the transform plane while the second mapping strategy is identical to a binary-weight magnitude-only SLM except for a shift in the dc level.[18] Objections to these limitations can also be addressed by considering the cascading of a magnitude-only SLM with the phase-only SLM, but this reduces the compactness that this example is designed to illustrate. The performance of the interferometer is also affected by the accuracy to which the phase of each pixel of the SLM is offset.

The correlation-plane response in Fig. 3 is also determined by interferometry, if we use the relationship that intensity is proportional to the sum of squares of I and Q. This is accomplished by the following steps. After the phase difference $\phi(i,j)$ is calculated the switch in Fig. 3 is set to direct this signal into the SLM. Three frames are intensity recorded with the constant phase shift, as before. The three frames are processed as shown in Fig. 1 to determine I and Q, which are further processed by a sum-of-squares circuit that is in parallel with the inverse-tangent circuit. While this way of calculating the correlation surface requires the recording of three frames, there is no need to turn off the reference beam. This therefore eliminates the need for a shutter when recording the correlation image. If the full complex SLM that is mentioned above is used, then the sum-of-squares circuit can also be used to program the magnitude-only portion of the tandem. For the Fig. 3 correlator to be adaptive in real time, nine frames per scene (three interferograms each for the scene, reference, and correlation planes) are required. Note that 4-kHz frame rates have been reported for recent 128 × 128 pixel DMD's,[19] which could be used to provide processing rates substantially in excess of standard video.

The polarizing beam splitter and the quarter-wave plate are included to overcome beam-splitter losses from the signal and reference beams. They also keep unwanted reflections from several surfaces from reaching the camera. In order to approach 100% collection of the light, some obscuration from the laser diode (of the reference beam) and from the small mirror (of the signal beam) is incurred. The reference beam can fill in around the laser diode by diffraction and spatial filtering of the mirror. The SLM illumination beam can also diffract around the small mirror, and the optical Fourier transform can smooth out some of the errors and interference from these secondary wavelets. A Mach–Zehnder implementation with no obscurations can be made also. A quarter-wave plate and a polarizing beam splitter behind the FBDMD can be used to recover the light reflected from the FBDMD. However (assuming a 50/50 beam splitter in front of the camera), only 50% of the signal and reference beams would reach the camera. Another half-wave plate would also be needed to align the polarizations of signal and reference beams.

Phase-Estimation Circuitry

A rough estimate of the serial rates required to calculate the phase is driven by the SLM frame rate and the number of SLM pixels. At 30 frames/s a 128 × 128 SLM sets a rate of $0.5(10^6)$ calculations/s

for the inverse-tangent circuit. If the fully time-shared architecture of Fig. 3 is used, then the calculation rate is increased by a factor of 9. Many groups have stated interest in pushing SLM's to 10^6-pixel resolution and 1-kHz frame rates, indicating that rates of 10^9 calculations/s might eventually be needed. (While the current 128 × 128 DMD addressing circuits achieve rates faster than this, scaling to 10^6-pixel SLM's will either run slower or require extremely large bandwidth serial-to-parallel demultiplexors.[20]) Imagers of similar resolution and frame rate would also be needed for these faster systems.

Analog or digital versions of the phase-estimation circuitry are possible, but we expect that the analog version would achieve the greatest speeds, the smallest size, and the lowest power dissipation. The all-digital approach would require the added costs of analog-to-digital and digital-to-analog convertors and arithmetic units. Digital division can be slow, while analog division can be done using log amplifiers. CCD arrays are envisioned as the frame memory for the I_i and ϕ_R in analog implementations. The memory for the three interferograms can be reduced to two frames by storing the data as $Z_1 = I_0 - I_1$ and $Z_2 = I_0 - I_2$. Equation (3) can be re-expressed in terms of these linearly transformed variables.

A block diagram of an analog implementation of the inverse-tangent circuit is shown in Fig. 4(a). The portion of the circuit inside the dashed box outputs values between 0 and $\pi/2$. The log amplifiers and the subsequent nonlinear amplifier together perform the division, the inverse-tangent function, and a $\pi/4$-level shift. The output of this last amplifier varies only between 0 and $\pi/4$, as plotted in Fig. 5. The third detection bit indicates whether the value output by this amplifier should be placed between $\pi/4$ and $\pi/2$ (for bit b_3 true) or between 0 and $\pi/4$ (for bit b_3 false). We used the result that the tangent is a symmetric reflection of the cotangent around $\pi/4$. This permits the same amplifier transfer function to be used to calculate either range of the phase. Bits 1 and 2 enable the phase to be placed in the proper quadrant. When determination of phase to 4 bits ($\pi/8$ resolution) is deemed adequate, then the circuit shown in the dashed box in Fig. 4(a) may be replaced by that shown in Fig. 4(b). In developing the high-accuracy phase-determination circuit [Fig. 4(a)] we may somewhat distort the nonlinearity to correct for systematic errors earlier in the circuit. Additional nonlinear amplifiers could follow the circuit in order to compensate for any nonlinear mapping of the voltage ϕ to the FBDMD pixel displacement. It is likely that there is an off-the-shelf circuit (for performing arbitrary γ correction of video cameras) that can be adjusted to approximate these various nonlinear amplifiers.

The multipliers in Fig. 4(a) could be implemented by switching between outputs of a complementary output device. A potentially simpler arrangement of the multiplier blocks and adders is shown in Fig. 4(c). The two adders can also be represented by a single four-position switch.

Dynamic Range of the Interferometer

We define the dynamic range of the interferometer as the ratio of the maximum possible optical amplitude a_{max} to the minimum amplitude a_{min} needed to measure phase ϕ to a given resolution Δ. It is limited by the ratio of the maximum intensity $I_{max} = (1 + a_{max})^2$ observed by the interferometer plane camera and its minimum detectible signal level σ (which we treat here as the standard deviation of a thermal noise-limited detector.) The camera signal-to-noise ratio $S/N = I_{max}/\sigma$ is considered to be equivalent to its dynamic range for this discussion.

The propagation of camera noise into the measurements of I and Q is found directly by evaluating the standard deviation of each part of Eq. (3) by the general formula

$$\sigma_x^2 = E[x^2] - E^2[x], \tag{5}$$

where $E[\ ]$ is the expectation operator. In the simplest case, in which each image I_i has the same standard deviation σ and in which the images I_i are uncorrelated with each other, the standard deviations of I and Q are

$$\sigma_I = \sqrt{\frac{3}{2}}\frac{\sigma}{1 - \cos\phi_1},$$
$$\sigma_Q = \sqrt{\frac{1}{2}}\frac{\sigma}{\sin\phi_1}. \tag{6}$$

If a phase shift ϕ_1 of $2\pi/3$ is used, then the measurements of I and Q are equally noisy, with standard deviations

$$\sigma_I = \sigma_Q = \sqrt{\frac{2}{3}}\sigma. \tag{7}$$

At angles of ϕ–Δ close to $\pi/2$, I is much smaller than Q and thus much more affected by measurement noise. Then, defining σ_I as the minimum detectible in-phase component, we can relate a_{min} to Δ by rearranging Eq. (3) as

$$a_{min} = \frac{\sigma_I}{2\cos(\pi/2 - \Delta)} = \frac{\sigma_I}{2\sin\Delta}. \tag{8}$$

Using the relationships in this section, including the specific result in Eq. (6), we can express the dynamic range of the interferometer as

$$\frac{a_{max}}{a_{min}} = \sqrt{6}\sin\Delta\frac{S}{N}\frac{a_{max}}{(1 + a_{max})^2}. \tag{9}$$

The maximum dynamic range D (when $a_{max} = 1$) is

$$D = \sqrt{\frac{3}{8}}\frac{S}{N}\sin\Delta, \tag{10}$$

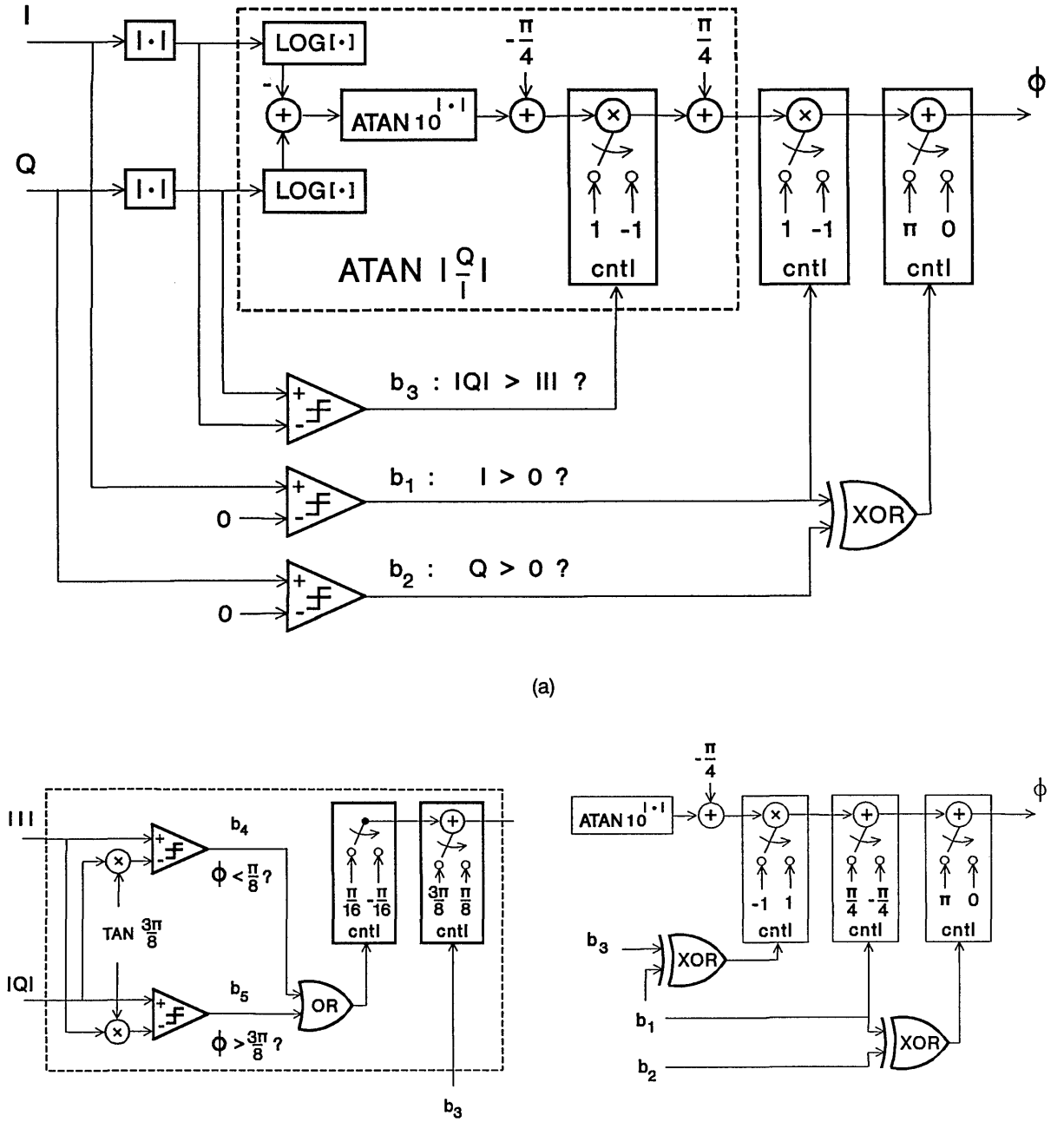

Fig. 4. Analog implementation of the inverse-tangent circuit: (a) Specific implementation using log amplifiers. Symmetry of the function is used to limit the dynamic range of the log amplifiers and the tan 10^x amplifier. The comparators determine in which octant of the unit circle that the phase lies, and the switching circuits place the phase in the correct octant. (b) Circuit that, when used in place of the ATAN $|Q/I|$ portion of (a), provides 4 bits of phase resolution. (c) Modifications to the right half of implementation (a) that reduce the number of multiplier units. All switches in the figure are shown set to the true state.

which is the main result desired. Many black-and-white cameras have advertised specifications for a S/N of from 200:1 to 1000:1 (46–60 dB), and CCD detector arrays have an ~80 dB S/N.[21] For a camera S/N of 1000:1, Eq. (9) indicates that the interferometer has a dynamic range of 60 for 6 bits of resolution ($\Delta_6 = 2\pi/64$) and 15:1 for 8 bits ($\Delta_8 = 2\pi/256$). In order to appreciate the sensitivity of the interferometer that has a S/N of 1000:1, note that it would be possible to measure the phase of a sinc function at the peak of its 19th sidelobe with a resolution of Δ_6 and the peak of its 5th sidelobe with a resolution of Δ_8.

The definition of dynamic range in Eq. (9) is somewhat arbitrary. A rough check of its validity is to evaluate the worst-case perturbation of ϕ to a

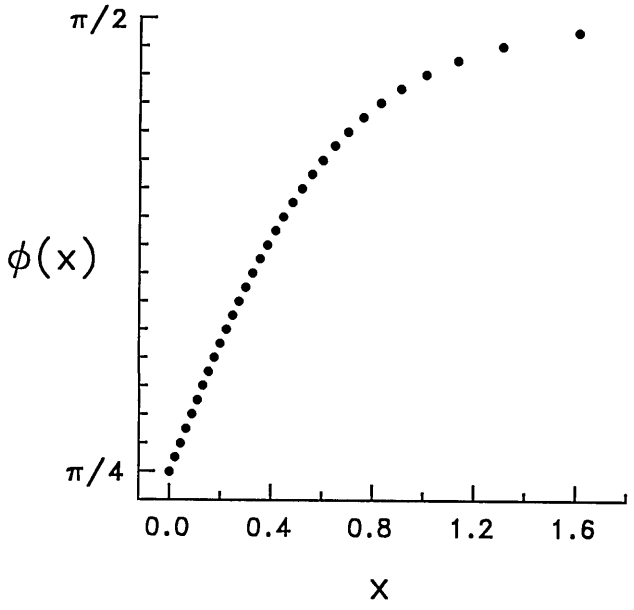

Fig. 5. Transfer function for a circuit with a nonlinearity of $\phi(x) = \tan^{-1} 10^x$. The curve shows samples of this function with a resolution of 8 bits on the unit circle (i.e., $\Delta_8 = 2\pi/256$).

one-standard-deviation error in I and Q; i.e.,

$$\phi + \delta\phi_{\pm} = \tan^{-1}\left[\frac{Q(a) \pm \sigma_Q}{I(a) \mp \sigma_I}\right], \quad a = a_{\min}. \quad (11)$$

For the case of phase-shift interval $\phi_1 = 2\pi/3$ the perturbation decreases from roughly $\pm 1.0\Delta$ to $\pm 1.4\Delta$ as ϕ decreases from $\pi/2$ to $\pi/4$ [which is the range of the $\tan^{-1}(10^x)$ circuit of Fig. 4(a)]. For the same numerical value of $a_{\min}$ but with $\phi_1 = \pi/2$ the perturbation is somewhat larger and between $3/2\Delta$ and $5/3\Delta$.

The analog circuitry must also have adequate performance to achieve the desired resolution. Approximating only one eighth of the unit circle, as described above, reduces the dynamic range required to calculate phase to the desired resolution Δ. For example, the dynamic range of Q/I is 8.3:1 over the range $\pi/4 + \Delta_6$ and $\pi/2 - \Delta_6$ and 39:1 over the range $\pi/4 + \Delta_8$ and $\pi/2 - \Delta_8$. The dynamic range of either I or Q would be larger than the dynamic range of I/Q by the factor D [see Eq. (9)]. Therefore either log amplifier must be able to handle a dynamic range of at least 500:1 for Δ_6 and 580:1 for Δ_8. The dynamic range of $\log(Q/I)$, which is the input of the $\tan^{-1}(10^x)$ circuit, is 12:1 for 6-bit resolution and 76:1 for 8-bit resolution. The dynamic range of the output of the $\tan^{-1}(10^x)$ circuit need not be much greater than that set by the achievable resolution. This calls for a dynamic range of 2^{n-3} to achieve a resolution of Δ_n. The dynamic range required is greatest for the log amplifiers, but still well within the performance limits of current video-rate analog components.

Discussion

This discussion is intended to further clarify the distinctions and trade-offs in using one specific implementation of an adaptive real-time correlator over another. This includes some comparisons with the JTC.

The general adaptive phase-only architecture (Fig. 1) can be implemented to run with an internal frame rate identical to scene frame rate but at the exorbitant cost of using six identical interferometers. To overcome these obvious objections, we considered ways to make the specific implementations more compact while maintaining adaptivity and large diffraction efficiencies.

Figure 2 shows the first step in this direction. Here a single interferometer is time shared to record the six interferograms. This architecture requires only two SLM's and a phase shifter. The architecture may also be extended to measuring the full complex modulation (by additionally calculating the magnitude of the spectrum from I and Q, as in the circuit shown in Fig. 3) and full complex filtering by cascading the transmittance of the phase-only SLM with a magnitude-only SLM. Thus real-time phase detecting and phase-modulating devices permit the calculation of the true correlation integral without the added nonlinearly generated terms that have become accepted nuisances since the invention of the VanderLugt correlator.

The implementation in Fig. 3 is the most compact version of the correlator. It requires a single phase-only SLM, which also serves as a phase modulator and approximates an amplitude modulator. Obviously, performance is sacrificed in using the SLM to represent a binary amplitude version of the analog intensity scene, but the reduction in optical hardware and the ruggedness possible with a common-path interferometer may outweigh this objection in applications involving high-vibration environments or small autonomous vehicles.

Another sacrifice in either the Fig. 2 or Fig. 3 implementations is the increased electronic bandwidth of six to nine times over fully parallel correlator architectures. Nor is this the first time that such a trade-off has been made. Consider that, in adaptive real-time operation, the compact JTC requires an internal bandwidth of at least twice the video bandwidth of the scene. This becomes three times the scene bandwidth if both the scene and reference images are recorded sequentially; for instance, to eliminate an extra camera. These added bandwidth requirements along with the relative complexity of performing the inverse-tangent operation indicate the need for an analog, rather than digital, numeric approach. We envision that an integrated video circuit can be developed to perform the arctangent function serially.

It is worth noting that electronic evaluation of the correlation surface for pattern-recognition and tracking applications need be performed only at the scene frame rate. Whether specific correlation-plane electronics can keep up with scene frame rates more than the standard 30 frames/s is not addressed here, but we are confident that substantially faster rates can be

achieved; if not with a central processing unit, then with circuitry specifically designed for the intended application.

Conclusions

We have presented a new architecture for performing optical pattern recognition with phase-only correlation. Perhaps its most novel feature is that the Fourier-plane phase of the signal and reference images is subtracted electronically rather than optically.

Using a real-time phase-measuring interferometer makes it possible to program the filter plane of the phase-only correlator with live scenery. The phase-only correlator can thus demonstrate adaptivity in real-time comparable with the JTC and is capable of much greater light utilization efficiency than the JTC. A physically compact version of the optical system can be built that uses a single SLM and a Fourier-transform lens. However, the performance of this compact system may be reduced somewhat owing to partial obscurations and to the nonlinear mapping of the signal to the phase-only image-plane light modulator. Nonetheless, high-efficiency utilization of light and mechanical stability owing to common-path interferometry are possible. Current analog electronics and cameras appear to have the dynamic range and the bandwidth needed for highly resolved phase determination at serial video rates.

I am indebted to A. C. Parola and D. V. Cohn of the University of Louisville for introducing me to and instructing me on the use of the software used to generate the figures in this study.

References and Notes

1. A. VanderLugt, "Signal detection by complex spatial filtering," IEEE Trans. Inf. Theory **IT-10,** 139–145 (1964).
2. F. T. S. Yu, S. Jutamulia, T. W. Lin, and D. A. Gregory, "Adaptive real-time pattern recognition using a liquid crystal TV based joint transform correlator," Appl. Opt. **26,** 1370–1372 (1987).
3. C. S. Weaver and J. W. Goodman, "A technique for optically convolving two functions," Appl. Opt. **5,** 1248 (1966).
4. J. L. Horner, "Light utilization in optical correlators," Appl. Opt. **21,** 4511–4514 (1982).
5. J. L. Horner and P. D. Gianino, "Phase-only matched filtering," Appl. Opt. **23,** 812–816 (1984).
6. J. Knopp and S. E. Monroe, Jr., "Optical calculation of correlation filters," in *Real-Time Image Processing II,* R. D. Juday, ed., Proc. Soc. Photo-Opt. Instrum. Eng. **1295,** 68–75 (1990).
7. J. H. Bruning, D. R. Herriott, J. E. Gallagher, D. P. Rosenfeld, A. D. White, and D. J. Brangaccio, "Digital wave-front measuring interferometer for testing optical surfaces and lenses," Appl. Opt. **13,** 2693–2703 (1974). Also see J. H. Bruning, "Fringe scanning interferometers," in *Optical Shop Testing,* D. Malacara, ed. (Wiley, New York, 1978), Chap. 13. A more recent source is J. Schwider, R. Burrow, K.-E. Elssner, J. Grzanna, R. Spolaczyk, and K. Merkel, "Digital wave-front measuring interferometry: some systematic error sources," Appl. Opt. **22,** 3421–3432 (1983).
8. K. K. Clarke and D. L. Hess, *Communication Circuits: Analysis and Design,* (Addison-Wesley, Reading, Mass., 1971), Chap. 12.
9. For further discussion on magnitude phase tandems, see D. A. Gregory, J. C. Kirsch, and E. C. Tam, "Full complex modulation using liquid-crystal televisions," Appl. Opt. **31,** 163–165 (1992).
10. J. Amako and T. Sonehara, "Kinoform using an electrically controlled birefringent liquid-crystal spatial light modulator," Appl. Opt. **30,** 4622–4628 (1991), and references therein.
11. K. Lu and B. E. A. Saleh, "Complex amplitude reflectance of the liquid-crystal light valve," Appl. Opt. **30,** 1374–1378 (1991).
12. L. J. Hornbeck, "Deformable-mirror spatial light modulators," in *Spatial Light Modulators and Applications III,* U. Efron, ed., Proc. Soc. Photo-Opt. Instrum. Eng. **1150,** 86–102 (1989).
13. R. M. Boysel, J. M. Florence, and W. R. Wu, "Deformable mirror light modulators for image processing," in *Optical Information Processing Systems and Architectures,* B. Javid, ed., Proc. Soc. Photo-Opt. Instrum. Eng. **1151,** 183–194 (1989).
14. J. M. Florence, Texas Instruments, Dallas, Tex. 75265, and J. L. Horner, Rome Air Development Center, Hanscom Air Force Base, Mass. 01731-5000 (personal communication).
15. D. A. Gregory, R. D. Juday, R. Gale, J. B. Sampsell, R. W. Cohn, and S. E. Monroe, Jr., "Optical characteristics of a deformable mirror spatial light modulator," Opt. Lett. **13,** 10–12 (1988).
16. J. M. Florence, "Joint-transform correlator systems using deformable-mirror spatial light modulators," Opt. Lett. **14,** 341–343 (1989).
17. K. H. Fielding and J. L. Horner, "1-f binary joint transform correlator," Opt. Eng. **29,** 1081–1087 (1990).
18. More on distinctions between binary phase-only and binary magnitude-only modulation is found in M. A. Flavin and J. L. Horner, "Amplitude encoded phase-only filters," Appl. Opt. **28,** 1692–1696 (1989).
19. R. M. Boysel, "A 128 × 128 frame-addressed deformable mirror spatial light modulator," Opt. Eng. **30,** 1422–1427 (1991).
20. For instance, consider the addressing circuit schematics in Refs. 12 and 19.
21. E. L. Deraniak and D. G. Crowe, *Optical Radiation Detectors* (Wiley, New York, 1984), Chap. 9.